Rendering Dynamic Source Motion in Surface Haptics via Wave Focusing

Gregory Reardon[1], Dustin Goetz[2], Max Linnander[2], and Yon Visell[3]

***Abstract*—Emerging surface haptic technologies can display localized haptic feedback anywhere on a touch surface by focusing mechanical waves generated via sparse arrays of actuators. However, rendering complex haptic scenes with such displays is challenging due to the infinite number of physical degrees of freedom intrinsic to such continuum mechanical systems. Here, we present computational focusing methods for rendering dynamic tactile sources. They can be applied to a variety of surface haptic devices and media, including those that exploit flexural waves in thin plates and solid waves in elastic media. We describe an efficient rendering technique based on time-reversal of waves emitted from a moving source, and motion path discretization. We combine these with intensity regularization methods that reduce focusing artifacts, improve power output, and increase dynamic range. We demonstrate the utility of this approach in experiments with a surface display that uses elastic wave focusing to render dynamic sources, achieving millimeter-scale resolution in experiments. Results of a behavioral experiment show that participants could readily feel and interpret rendered source motion, attaining 99% accuracy across a wide range of motion speeds.**

***Index Terms*—Surface Haptics, Source Rendering, Wave Focusing, Tactile Motion**

I. INTRODUCTION

A major challenge in haptics is to engineer displays that can render spatiotemporal haptic scenes that are specified in software media, rather than being pre-determined by the physical configuration of the device and actuators. Emerging technologies for mid-air haptics [1], [2] and surface haptics [3], [4], [5] employ arrays of remotely positioned actuators to focus solid or aeroacoustic mechanical waves at arbitrary, software-specified locations in space, yielding localized haptic sensations that are perceived as virtual sources of tactile feedback. Such technologies could make it possible to achieve a longstanding goal in haptics – that of realizing practical, general-purpose haptic displays that can render arbitrary dynamic haptic scenes specified as digital media content, in much the same way that high-fidelity computer graphics and spatial sound rendering can be accomplished today.

However, rendering haptic feedback via wave focusing is challenging because the manner in which mechanical signals are furnished is indirect, mediated by the wave physics of a continuum mechanical medium with infinitely many degrees of freedom. In general, rendering requires that one solve a high-dimensional inverse problem of determining driving signals for a sparse array of actuators that yield a distributed wave field approximating a specified haptic scene to be rendered, at all locations and times of interest. In ultrasound-based mid-air haptics, this problem can be solved using standard phased-array techniques that exploit the relatively idealized nature of acoustic propagation in air [1], [2].

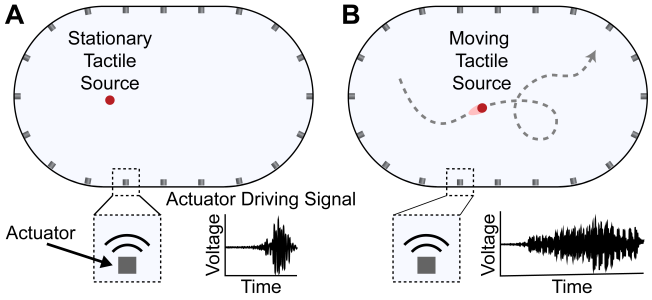

Fig. 1. Our computational wave-focusing method can render stationary (A) or dynamic (moving) tactile sources (B), and can be applied to a variety of different media and systems. The method is based on source motion time-reversal focusing using experimentally measured Green's functions captured from the system.

In wave-focusing-based surface haptics, which is treated in this paper, rendering problems involve one fewer space dimension. However, this simplification is more than offset by other prominent physical complications that are common to such displays, such as non-idealized boundary conditions, medium heterogeneity, energetic losses due to internal friction, and complex, geometry-dependent modal behaviors. Nonetheless, several methods for dynamically controlling the localization or distribution of haptic feedback provided via actuated surfaces have been reported during the past several years.

Inverse filtering methods utilize transfer function matrices obtained from measurements and can focus surface waves concentrated at one or more control locations [4], [6]. Other methods derive solutions in terms of eigenfunctions [7]. Confinement techniques exploit physical effects in engineered surfaces that impede the transmission of wave components at some frequencies, yielding feedback that can be localized or confined within particular domains of a surface [8], [9], albeit in a manner that depends on hardware design choices.

Time-reversal focusing refers to a family of techniques that exploit approximate physical symmetries, including time-reversal and reciprocity, to focus waves in arbitrary propaga-

[1]Gregory Reardon is with Media Art and Technology Program, University of California, Santa Barbara, CA 93106 USA reardon@ucsb.edu

[2]Dustin Goetz and Max Linnander are with the Department of Mechanical Engineering, University of California, Santa Barbara, CA 93106 USA dgoetz@ucsb.edu, maxlinnander@ucsb.edu

[3]Yon Visell is with the Biological Engineering Program and Department of Mechanical Engineering, University of California, Santa Barbara, CA 93106 USA yonvisell@ucsb.edu

Manuscript received XXX; revised XXX.

tion media [10]. They can be computationally efficient, but are often data-intensive, requiring direct measurements of the Green's functions encoding physical transmission from each actuator to each possible focus location. Such approaches have been used in surface haptics for delivering localized tactile feedback by focusing flexural waves in thin plates [3], and (in prior research by the authors) for delivering single- and multi-point localized feedback by focusing viscoelastic waves in a soft plate [5].

Despite progress, existing display methods based on wave focusing cannot yet render a wide range of dynamic haptic scenes. Here, we treat dynamic haptic scenes that are composed of moving sources of tactile feedback. For clarity, the sources are mechanical signals concentrated at specified, time-varying locations, rather than localized percepts, illusions, or sensations of motion produced via relocalization, funneling, or apparent motion [11], [12], [13].

In Section II, we first derive a method for dynamic source rendering based on time-reversal of waves emitted from a moving source. The source is specified by an arbitrary time-varying mechanical signal $u(t)$ that excites localized oscillations in the medium as it travels along a path $\boldsymbol{p}(t)$ of surface coordinates (Fig. 1). We then derive an approximate rendering method, based on motion path discretization, that is amenable to practical implementation. Motivated by limitations in focusing fidelity that arise due to variations in focal location, we augment our rendering method with intensity regularization factors that reduce focusing artifacts, improve power output, and that increase dynamic range in some settings. These methods can be applied to surface haptic devices that employ a variety of media and physical processes, including those exploiting flexural waves in thin plates or solid waves in elastic media. We demonstrate the utility of these methods in experiments with a surface display that focuses elastic waves using an array of electromagnetic actuators, rendering dynamic tactile sources with millimeter-scale resolution. We also report the results of a perceptual experiment on the discrimination of the direction of source motion felt by multiple fingertips. We found that users could accurately perceive the direction of motion of rendered sources, attaining 99% accuracy across a wide range of motion speeds (4 cm/s to 50 cm/s).

II. Rendering Dynamic Source Motion

Our method for rendering dynamic tactile sources traveling along surface paths builds on, and extends, prior techniques for synthesizing localized tactile sources in surface haptics.

A. Surface haptic wave focusing

Focusing involves rendering spatially localized displacement wave fields $\boldsymbol{y}(\boldsymbol{x},t)$, where variables in bold signify vectors, via an array of N discrete actuators positioned at surface locations $\boldsymbol{z}_i$, $i = 1,2,\ldots,N$. Each ith actuator delivers a localized force signal $\boldsymbol{f}_i(t)$ that excites the medium. Approximating the actuators as point sources, $\boldsymbol{y}(\boldsymbol{x},t)$ satisfies

$$L\,\boldsymbol{y}(\boldsymbol{x},t) = \sum_{i=1}^{N} \boldsymbol{f}_i(t)\delta(\boldsymbol{x}-\boldsymbol{z}_i), \tag{1}$$

where L is a linear hyperbolic differential operator encoding the physics of the system. For flexural waves in a thin plate, L has the form

$$L = -\rho h\frac{\partial^2}{\partial t^2} + D\nabla^2\,, \quad D = \frac{Eh^3}{12(1-\nu^2)} \tag{2}$$

where the displacement is scalar-valued, $y(\boldsymbol{x},t)$, D is the flexural stiffness, E is the plate Young's modulus, ν is Poisson's ratio, ρ is mass density, and h is the plate thickness.

For solid elastic waves, L has the form

$$L = -\rho\frac{\partial^2}{\partial t^2} + \mu\nabla^2 + ((K+\mu/3)\boldsymbol{\nabla})\boldsymbol{\nabla}\cdot \tag{3}$$

Here, ρ is again the mass density, μ is the shear modulus, and K is the bulk modulus. For viscoelastic waves, the elastic medium is damped and dispersive, and the propagation speed $c(\omega)$ and damping both depend on frequency $\omega = 2\pi f$ [14], [15], [16].

Formal solutions, with suitable boundary conditions, may be efficiently expressed via Green's functions $g_i^{\alpha\beta}(\boldsymbol{x},t)$ that describe oscillations of the medium produced by a force impulse from the ith actuator, where α and β index the force and oscillation directions. For scalar waves, or when only one direction each of actuation and oscillation is of interest, solutions are described by a scalar expression

$$y(\boldsymbol{x},t) = \sum_{i=1}^{N} g_i(\boldsymbol{x},t) * f_i(t), \tag{4}$$

where $*$ denotes convolution in time. (For clarity, we treat the scalar case in the rest of the paper.) Focusing involves solving the inverse problem of determining driving forces $f_i(t)$ that yield a specified spatiotemporal wave field $y(\boldsymbol{x},t)$.

When measurements (or an accurate model) characterizing the system are available, focusing can be performed using the time-reversal method [10]. To render an impulsive tactile source that is instantaneously localized near an arbitrary location $\boldsymbol{x}_0$, one first measures the Green's functions $\hat{g}_i(\boldsymbol{x}_0,t)$ from the actuator to source locations. After time-reversal, the driving force signals are given by $f_i(t) = \hat{g}_i(\boldsymbol{x}_0, T-t)$, where T is the focusing time. The focused wave field is given by

$$y(\boldsymbol{x},t) = \sum_{i=1}^{N} g_i(\boldsymbol{x},t) * \hat{g}_i(\boldsymbol{x}_0, T-t) \tag{5}$$

At $\boldsymbol{x} = \boldsymbol{x}_0$, the result approximates an idealized impulse $y(\boldsymbol{x}_0,t) \approx \delta(t-T)$. A source with arbitrary temporal waveform $u(t)$ may be rendered by supplementing the forces with a further convolution, $f_i(t) = \hat{g}_i(\boldsymbol{x}_0, T-t) * u(t)$. At the focus location $\boldsymbol{x}_0$, this yields $y(\boldsymbol{x}_0,t) \approx u(t-T)$. Passing to the Fourier transform domain, the focusing solution is

$$Y(\boldsymbol{x},\omega) = U(\omega)\sum_{i=1}^{N} G_i(\boldsymbol{x},\omega)\overline{\hat{G}}_i(\boldsymbol{x}_0,\omega)e^{j\omega T} \tag{6}$$

where $Y(\boldsymbol{x},\omega)$, $U(\omega)$, and $G_i(\boldsymbol{x},\omega)$ are the Fourier transforms of $y(\boldsymbol{x},t)$, $u(t)$, and $g_i(\boldsymbol{x},t)$. ($\overline{a}$ denotes the complex conjugate of a complex number a.)

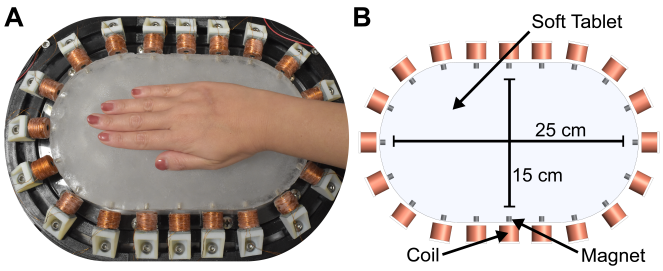

Fig. 2. A) We evaluated our rendering methods by displaying dynamic sources with a hardware system that focuses elastic waves in a soft plate with the dimensions shown. B) Waves are focused via forces applied by an array of coils to 20 magnets embedded within the plate periphery.

B. Dynamic source rendering

A dynamic source emits a signal $u(t)$ at each instant along a path, which is a spatiotemporal trajectory of surface coordinates $\boldsymbol{p}(t)$. We first analyze the physics governing wave transmission from a moving source to the actuator locations and then apply time-reversal and reciprocity to obtain the driving signals required for source rendering. First, consider a physical source that emits a single impulse $u(t) = u_0\,\delta(t-s_0)$ at time instant $t = s_0$ from corresponding path position $\boldsymbol{p}(s_0)$. Each ith actuator receives a "forward" signal $f_i^{\text{fwd}}(t)$ given by

$$f_i^{\text{fwd}}(t) = u_0\, g_i(\boldsymbol{p}(s_0), t - s_0) \tag{7}$$

where $t - s_0$ is the time elapsed since emission. An arbitrary source signal may be expressed as a sum of such impulses, $u(t) = \int_0^t ds\, u(s)\,\delta(t-s)$. The received signals are

$$f_i^{\text{fwd}}(t) = \int_0^t ds\, u(s)\, g_i(\boldsymbol{p}(s), t - s) \tag{8}$$

Applying time-reversal and reciprocity symmetry (exchanging source for receiver), the actuator driving signals required for rendering the dynamic source are

$$f_i(t) = \int_0^t ds\, u(s)\, \hat{g}_i(\boldsymbol{p}(s), T - t + s) \tag{9}$$

An analogous result, derived via other means, is reported in a theoretical paper by Garnier and Fink [17]. For a stationary source, $\boldsymbol{p}(t) = \boldsymbol{p}_0$, this expression reduces to a convolution between $u(t)$ and $g_i(\boldsymbol{p}_0, -t)$, which may be efficiently computed via Fourier transform. (For convenience, we hereinafter choose the time origin so that $T = 0$). For any realistic system, computing each driving signal requires numerical integration of (9). In many cases, this would be too computationally intensive for practical application.

C. Sampled path approximation

Consider points $\boldsymbol{p}_m = \boldsymbol{p}(t_m)$ sampled at regular intervals $t_m = m\Delta t$ along the source motion path. We can write

$$f_i(t) = \sum_{m=1}^{M} \int_{t_m}^{t_{m+1}} ds\, u(s)\, \hat{g}_i(\boldsymbol{p}(s), s - t) \tag{10}$$

Green's functions at nearby positions are often highly correlated (see Fig. 4D), so one can approximate $\hat{g}_i(\boldsymbol{p}(s), s-t) \approx \hat{g}_i(\boldsymbol{p}_m, s-t)$. Upon shifting the variable of integration, this yields

$$f_i(t) \approx \sum_{m=1}^{M} \int_0^{\Delta t} ds\, u(s + t_m)\, \hat{g}_i(\boldsymbol{p}(s), s - t_m) \tag{11}$$

Let $u_m(t) = u(t + t_m)$. If the decay time for the Green's function is shorter than Δt, then the approximation (11) for the actuator driving signal is equal to a sum of convolutions

$$f_i(t) \approx \sum_{m=1}^{M} u_m(t) * \hat{g}_i(t_m - t) \tag{12}$$

This approximation describes a setting in which focusing causes each excitation $u_m(t)$ to be independently emitted from each source location $\boldsymbol{p}_m$. The Fourier transform $F_i(\omega) = \mathcal{F}\{f_i(t)\}$ is

$$F_i(\omega) = \sum_{m=1}^{M} U_m(\omega)\overline{\hat{G}}_i(\boldsymbol{p}_m, \omega)\, e^{j\omega t_m} \tag{13}$$

Using Fourier convolution, the number of computations required to compute this approximation of $f_i(t)$, in discrete time, is $\mathcal{O}(ML\log L)$, where L is the number of discrete time samples, which depends on the physical medium, system implementation, including sample rate, and source to be rendered. In contrast, the exact expression (9) would require $\mathcal{O}(ML^2)$ discrete-time calculations, because the integral over s must be computed for each value of t. For illustration, taking representative values associated with the system of Sec. IV ($L \sim 10^3$; $M, N \sim 10^1$), the sequential approximation requires $\sim 10^3$ fewer calculations, making it far more amenable to practical implementation, and motivating its use in our experiments, described below.

D. Intensity regularization

One source of artifacts in time-reversal focusing arises because the actuator driving signals $f_i(t)$ are larger in amplitude for actuators that are nearer to the focus location. This impairs focal quality, decreases power output, and reduces dynamic range. To mitigate such effects, we introduce a focus location-dependent saturating gain factor $\sigma_i(\boldsymbol{x}_0)$ that multiplies the output amplitude from each actuator:

$$\sigma_i(\boldsymbol{x}_0) = \begin{cases} 1 & \hat{g}_i(\boldsymbol{x}_0)_{RMS} < C \\ C\,\hat{g}_i(\boldsymbol{x}_0)_{RMS}^{-1} & \text{else} \end{cases} \tag{14}$$

where $\hat{g}_i(\boldsymbol{x}_0)_{\text{RMS}}$ is the RMS amplitude of $\hat{g}_i(\boldsymbol{x}_0, t)$, and C is a saturation threshold that may be tuned. (Saturation decreases as C increases.)

Wave focusing often exhibits focus-location-dependent amplitude variations due to physical damping, geometry effects, or other phenomena. To avoid such effects in dynamic source rendering, we introduce a gain factor, $n(\boldsymbol{x}_0)$ that normalizes amplitude at the respective focus location,

$$n(\boldsymbol{x}_0) = \left(\sum_{i=1}^{N} \sigma_i(\boldsymbol{x}_0) R_i(0) \right)^{-1} \tag{15}$$

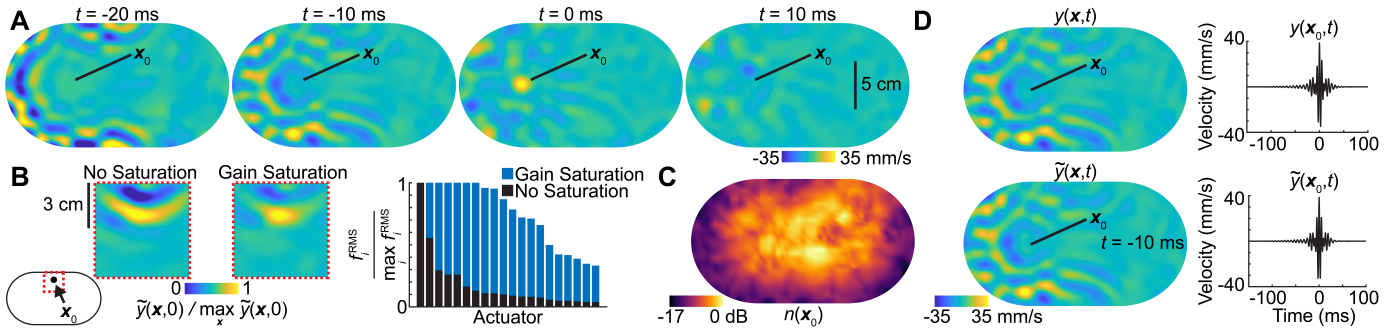

Fig. 3. A) Results of single-point focusing experiment. Time-reversal focusing causes energy to converge onto the specified focus location before it rapidly decays. B) Left: Wave field at focus time with and without saturation active. Right: Relative RMS actuator driving signal amplitudes with and without saturation. C) Focus gain normalization factors, $n(\boldsymbol{x}_0)$, obtained for focus locations $\boldsymbol{x}_0$ everywhere on the surface. Applying these gain factors compensated for variations in peak focus amplitude between locations. The relative gain in center regions was up to 17 dB greater than at the periphery, near the actuators. D) Representative focused wave fields obtained via optical vibrometry, $y(\mathbf{x}, t)$, and via convolution with the measured Green's function. The spatial distribution of oscillations (left) and their temporal waveforms (right) was nearly indistinguishable in all examined cases.

Here, $R_i(\tau)$ is the temporal autocorrelation of $g_i(\boldsymbol{x}_0, t)$. It is straightforward to show that $R_i(0)$ approximates the peak amplitude of the wave field at the focus location $\boldsymbol{x}_0$ and focus time. Including both regularization factors, the driving force signals for sampled path source rendering are given by

$$f_i(t) = \sum_{m=1}^{M} n(\boldsymbol{p}_m)\, \sigma_i(\boldsymbol{p}_m)\, u_m(t) * \hat{g}_i(\boldsymbol{p}_m, t_m - t) \qquad (16)$$

III. Experimental Platform

We demonstrate our rendering method in experiments with a surface haptic display that exploits wave focusing in a soft viscoelastic medium (Fig. 2A). The surface is a custom-fabricated, soft elastic plate (Gelatin #2, Humimic, USA) with a Bunimovich stadium cross-section (25 × 15 × 1.3 cm; see Fig. 2B) that is supported by a solid acrylic slab (thickness: 1.3 cm) bolted to a vibration isolated table. Plate oscillations are excited via in-plane forces delivered by an array of 20 coils (diameter: 2 cm, length: 1.5 cm, resistance: 14 ohms, inductance: 5 mH, 950 turns) driving each of 20 permanent magnets embedded near the edge of the elastic plate (NdFeB, diameter: 5 mm, length: 5 mm) yielding forces of up to 0.25 N each. The driving forces $f_i(t)$ are provided as amplified voltage signals (bandwidth 20 Hz - 24 kHz) exciting the coils. The audio signals are generated via desktop computer and commodity multichannel audio hardware. Further details regarding the engineering, design, and fabrication of the device are reported in a separate publication of the authors [18].

We characterized the system, and obtained results in our focusing experiments, by measuring plate oscillations that were excited via the driving force signals $f_i(t)$. Oscillations along the normal direction of the plate were imaged using a scanning laser doppler vibrometer (VPI 121, Ometron Ltd., UK), custom software, and a data acquisition unit (NI USB-6011; sample rate 10 kHz). We measured plate oscillations at each of 1500 surface locations $\boldsymbol{x}$ distributed across a grid with 4 mm spacing. This spatial sample resolution avoided aliasing by ensuring that the spatial Nyquist criterion was satisfied for driving frequency components up to 500 Hz, as assessed using results from our prior experiments with this material substrate [5]. The wave field oscillations $y(\boldsymbol{x}, t)$ captured in each experimental trial thus comprised an ensemble of 1500 time domain signals.

To facilitate wave focusing, we used the same instrumentation to measure Green's functions $\hat{g}_i(\boldsymbol{x}, t)$ from each ith actuator to each of the 1500 surface locations $\boldsymbol{x}$. Green's functions were measured using a sinusoidal frequency-sweep deconvolution method (20 to 500 Hz; 3 seconds; average over 3 trials). Their durations were brief (200 ms) due to viscoelastic damping. The measured Green's functions consisted of $3 \times 10^4 = 1500 \times 20$ time-domain signals, $\hat{g}_i(\boldsymbol{x}, t)$. Capturing these signals required 30 hours of continuous measurement.

Excited waves in the plate traveled in a frequency-dependent manner with a group velocity of approximately 4.8 m/s (estimated via bandlimited Dirac impulse transit time analysis), consistent with the authors' prior characterizations of waves in this substrate [19]. All results reported in the present paper are in the subsonic regime. Waves in the plate propagated with distance-dependent attenuation. Attenuation was approximately -3.8 dB/cm for bandlimited impulse driving signals (50-450 Hz).

IV. Rendering Results

A. Focusing with intensity regularization

We first evaluated the performance of the system, and the effects of intensity regularization, when focusing a brief impulse, $u(t)$, at individual (fixed) locations. During focusing, plate oscillations converged toward the specified focus location, $\boldsymbol{x}_0$, where they peaked in amplitude at the focus time $t = T$ (Fig. 3A). At later times $t > T$, the focused waves diverged, decaying over tens of milliseconds.

When gain saturation was not applied ($\sigma_i(\boldsymbol{x}_0) \equiv 1$), focusing to a location near any actuator yielded prominent diffraction artifacts (Fig. 3B), because the input was dominated by a single actuator (Fig. 3B, right panel, black). When gain saturation was applied, energy was distributed more uniformly among the actuators (Fig. 3B, right panel, blue), and focusing artifacts were greatly diminished. Gain normalization compensated for variations in the peak amplitude, $y(\boldsymbol{x}_0, T)$,

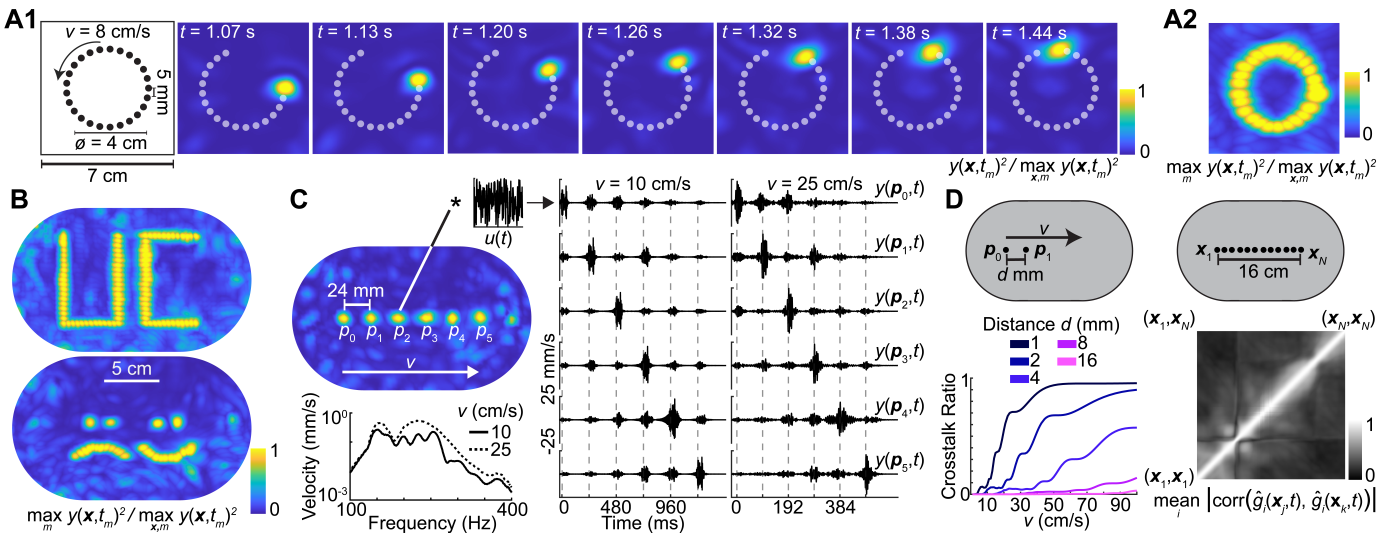

Fig. 4. A) Results of source rendering for a circular motion path (v = 8 cm/s), captured at successive focus times t_m (A1). Maximum amplitude across all focus times (A2). B) Results of rendering for source motion paths tracing letters (top frame) and emojis (bottom frame). Motion speed v = 8 cm/s (maximum across all focus times shown). C) Top Left: Rendered motion for a linear path sampled at six instants (speed v = 25 cm/s). Right: Excited wave oscillations $y(\boldsymbol{p}_m, t)$ at the sampled path locations. Dashed lines mark path sample instants t_m. Excitation signals $u(t)$ were white noise bursts. For speed $v = 10$ cm/s, the burst duration was 50 ms. For $v = 25$ cm/s, the burst duration was 15 ms. Bottom Left: Average magnitude spectrum of oscillation velocity at the sampled path locations. D) Crosstalk ratio (Sec. IV.C) as a function of motion speed v and path sample distance d. Coarser path discretizations permitted faster source motion without crosstalk, because the increased lag time reduced temporal overlap and the increased distance decreased correlations between the Green's functions (right panel).

of the focused wave field irrespective of the specified focus location $\boldsymbol{x}_0$. The gain normalization factors, $n(\boldsymbol{x}_0)$, depended on the focus location, and varied in a complex fashion across the plate (Fig. 3C). Values of $n(\boldsymbol{x}_0)$ near the center of the plate, far from the actuators, were up to 17 dB larger than those near the plate periphery, due to distance-dependent attenuation and other effects. When used, gain normalization ensures that the peak-to-peak amplitude at the focus does not vary with position, within measurement limitations. However, whereas $\sigma_i(\boldsymbol{x}_0)$ increases dynamic range when used, $n(\boldsymbol{x}_0)$ decreases dynamic range at locations near the periphery of the display, since peak amplitudes in center regions constrain those near the periphery.

B. Measurement fidelity and numerical experiments

We next assessed the accuracy with which the measured Green's functions $\hat{g}_i(\boldsymbol{x}_0, t)$ approximated the physical Green's functions $g_i(\boldsymbol{x}, t)$ encoding the wave physics of the medium. We compared wave fields $y(\boldsymbol{x}, t)$ that we measured from the system while driving the actuators with waves $\tilde{y}(\boldsymbol{x}, t)$ that we obtained numerically by using our measured Green's functions in place of those representing the physical system in (5),

$$\tilde{y}(\boldsymbol{x}, t) = \sum_{i=1}^{20} \hat{g}_i(\boldsymbol{x}, t) * \hat{g}_i(\boldsymbol{x}_0, T - t)\,. \tag{17}$$

Due to the high fidelity of our Green's function measurements, the numerically determined wave fields we obtained by applying (17) were in excellent quantitative agreement with those we obtained from the physical system using optical vibrometry measurements (Fig. 3D). Spatial and temporal attributes were nearly indistinguishable in all experimentally assessed focusing cases. Furthermore, such a numerical experiment requires just seconds to compute, whereas capturing vibrometry measurements in a physical experiment requires several hours. Since both methods produced identical results, we employed the numerical approach in our remaining experiments.

C. Dynamic source rendering

We evaluated dynamic sources that we rendered via sequential sampling. The sources traced paths $\boldsymbol{p}_m = \boldsymbol{p}(t_m)$ on the plate surface (Fig. 4). Upon focusing, the excited plate oscillations faithfully represented the specified source trajectory (Fig. 4A, B, C), making it possible to render sources that traced lines, geometric shapes, letters, and emojis. Rendering quality was maximized when the path sample period Δt was large enough that waves from focusing at $\boldsymbol{p}_{m-1}$ decayed before those at $\boldsymbol{p}_m$ commenced, minimizing crosstalk interference between the excited waves. Interference occurs because the Green's functions for nearby locations are correlated (Fig. 4D, right). We measured crosstalk as a ratio of the integrated signal energy at location $\boldsymbol{p}_m$ that was contributed by focusing at all other path locations, $\boldsymbol{p}_{m'}$ $(m' \neq m)$ to the integrated signal energy from focusing at $\boldsymbol{p}_m$ (Fig. 4D, left). Crosstalk increased with increasing motion speed $v = |\dot{\boldsymbol{p}}(t)|$ or with decreasing sample distance $d = |\boldsymbol{p}_m - \boldsymbol{p}_{m-1}|$. For $d = 4$ mm, crosstalk was negligible for $v < 16$ cm/s, which corresponds to $\Delta t > 25$ ms. Thus, rendering sources with finer spatial sampling required lower motion speeds. At sampling distances $d \geq 16$ mm, crosstalk was negligible for speeds up to 100 cm/s ($\Delta t > 16$ ms). In these conditions, the focal resolution ranged from 7 mm to 10 mm, as measured by the full-width at half-maximum at the focus.

V. Perception of Source Motion

We conducted a proof-of-concept perception experiment to illustrate the ability of our rendering method to render source motion that could be readily felt and interpreted without training. Participants reported the direction of motion of rendered sources that moved across the surface below their fingertips. Motion speed was varied in the experiment. The protocol was approved by the human subjects review board at the authors' institution. There were nine participants (ages 23 to 31, 4 female, 5 male), all of whom gave their written, informed consent.

Participants lightly touched the interface surface at six equally-spaced, specified positions along a 12 cm path using digits 2 to 4 of both hands (d = 24 mm; Fig. 5A). In each trial, they felt a source that moved left-to-right or right-to-left along the path at one of four speeds, v = 4, 10, 25, and 50 cm/s. Stimuli at each speed and direction were presented 10 times during the experiment, in randomized order. We replayed the source for the respective speed 1, 2, 3, or 4 times, after a 1-second pause, to approximately compensate for the shorter duration of higher speed stimuli. The source excitation signals $u_m(t) = u(t)$ were white noise bursts or (at the fastest speed) brief impulses. The amplitude of waves at the sampled path locations at focus times t_m averaged across speeds was 19.7 μm. Stimulus energy was concentrated in a band from 150 to 300 Hz. Fig. 4C shows the waveforms at the sampled path locations for v = 10 and 25 cm/s. Participants listened to pink noise via noise-canceling circumaural headphones during the experiment, provided responses verbally, and could request stimuli to be repeated, but rarely did so. For familiarization with the device and procedure, participants felt all 8 stimuli before the experiment began, but were not informed of the motion direction.

Participants reported the correct motion direction in 99% of all trials (713 out of 720). Every participant responded with greater than 95% accuracy. Response accuracy for speeds of 4, 10, 25, and 50 cm/s was 100%, 99.4%, 100%, and 96.7% respectively (Fig. 5B). The high accuracies preclude meaningful statistical analysis. In a post-experiment written survey, participants described the task as "very easy", and described the motion cues as "very clear." Faster stimuli were described as a pleasant "brush" across the fingertips, or as having greater "spatial continuity."

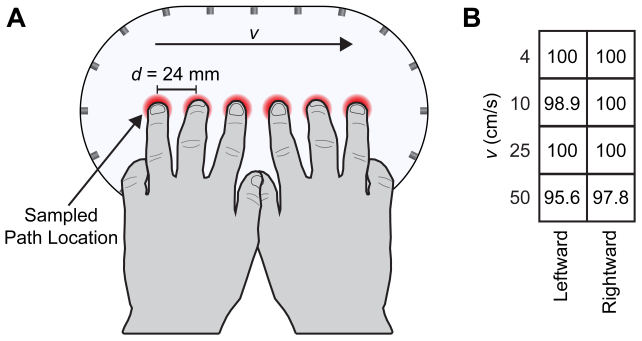

Fig. 5. A) Perceptual experiment on source motion. Sources moving with different speeds v were rendered along a surface path touched by the fingertips of digits 2 to 4 of both hands of the participant. B) Results of the experiment (mean accuracy percent for each speed and direction) indicate that source motion was accurately perceived.

VI. Conclusion

This paper presents an efficient computational method for rendering dynamic tactile sources in wave-focusing haptic displays. The method is based on the time-reversal of oscillations emitted from a moving source, and a path sampling approximation whose efficiency makes it amenable to practical application. We introduced intensity regularization factors that ensure consistent amplitudes throughout the surface, reduce artifacts by balancing actuator usage, and improve dynamic range, depending on system details.

We demonstrated these methods using an experimental platform consisting of a surface haptic device that employs an array of 20 electromagnetic actuators to excite, and focus, viscoelastic waves in a soft material medium. In focusing experiments, this device achieves millimeter-scale focal resolutions. Dynamic source rendering experiments yielded results in which focused waves reproduced source motion paths that traced simple or complex figures. The experiment highlighted how artifacts, including crosstalk, depended on tradeoffs between motion speed, path sampling resolution, and oscillation decay times and modal characteristics. The latter may vary greatly for other materials and systems. Thus, similar analyses would be appropriate if our method were to be applied to a different physical system, such as one based on flexural waves in thin plates.

The results we obtained reflected the linearity of the system in the regime in which it was driven. While we emphasized the rendering of individual dynamic sources, due to superposition, the same methods may be used to render multiple moving sources, or dynamic extended sources, via additive superposition of the driving signals.

The high-resolution optical vibrometry measurements used here to characterize our rendering method precluded the simultaneous loading of the haptic surface by the skin, which could, in principle, alter wave transmission. Further research on the complex effects of interfacial contact, which depend on contact geometry and the material and mechanical properties of the coupled skin and substrate, and their implications for wave transmission and focusing, may be merited, as exemplified in prior research on surface haptics [8]. Regardless, participants in our perceptual experiment accurately perceived the rendered source motion at all speeds.

Despite the simplicity of the behavioral experiment, it demonstrates the efficacy of the dynamic source motion rendering method reported here. Our perceptual results, obtained from participants who had no prior exposure or experience with rendered source motion, were consistent with our theoretical analyses and high-resolution vibrometry characterizations of wave focusing. In addition, participants described the stimuli as feeling brush-like and having greater "spatial continuity" as the source motion speed increased, as would be expected for moving sources with discretized motion paths. Nonetheless, further investigations on the perception of mov-

ing sources presented via wave-mediated haptic displays, and the experiences they can engender, including relationships to haptically perceived objects or events, are needed. Research on the perceptual influences of focusing parameters, system characteristics, and conditions of skin-surface contact would also be valuable.

ACKNOWLEDGEMENTS

We acknowledge the use of the UCSB CNSI Innovation Workshop and Microfluidics Facilities. This work was supported by NSF awards No. 1751348 to YV and No. 2139319 to DG.

REFERENCES

[1] T. Hoshi, M. Takahashi, T. Iwamoto, and H. Shinoda, "Noncontact tactile display based on radiation pressure of airborne ultrasound," *IEEE Transactions on Haptics*, vol. 3, no. 3, pp. 155–165, 2010.

[2] T. Carter, S. A. Seah, B. Long, B. Drinkwater, and S. Subramanian, "Ultrahaptics: multi-point mid-air haptic feedback for touch surfaces," in *Proceedings of the 26th annual ACM symposium on User interface software and technology*. ACM, 2013, pp. 505–514.

[3] C. Hudin, J. Lozada, and V. Hayward, "Localized tactile feedback on a transparent surface through time-reversal wave focusing," *IEEE Transactions on Haptics*, vol. 8, no. 2, pp. 188–198, 2015.

[4] L. Pantera and C. Hudin, "Multitouch vibrotactile feedback on a tactile screen by the inverse filter technique: vibration amplitude and spatial resolution," *IEEE transactions on haptics*, vol. 13, no. 3, pp. 493–503, 2020.

[5] G. Reardon, N. Kastor, Y. Shao, and Y. Visell, "Elastowave: Localized tactile feedback in a soft haptic interface via focused elastic waves," in *2020 IEEE Haptics Symposium (HAPTICS)*. IEEE, 2020, pp. 7–14.

[6] L. Pantera, C. Hudin, and S. Panëels, "Lotusbraille: Localised multi-finger feedback on a surface for reading braille letters," in *2021 IEEE World Haptics Conference (WHC)*. IEEE, 2021, pp. 973–978.

[7] J.-H. Woo and J.-G. Ih, "Vibration rendering on a thin plate with actuator array at the periphery," *Journal of Sound and Vibration*, vol. 349, pp. 150–162, 2015.

[8] A. B. Dhiab and C. Hudin, "Confinement of vibrotactile stimuli in narrow plates: principle and effect of finger loading," *IEEE Transactions on Haptics*, vol. 13, no. 3, pp. 471–482, 2020.

[9] T. Daunizeau, D. Gueorguiev, S. Haliyo, and V. Hayward, "Phononic crystals applied to localised surface haptics," *IEEE Transactions on Haptics*, vol. 14, no. 3, pp. 668–674, 2021.

[10] M. Fink, "Time reversal of ultrasonic fields. I. basic principles," *IEEE Transactions on Ultrasonics, Ferroelectrics, and Frequency Control*, vol. 39, no. 5, pp. 555–566, 1992.

[11] G. von Békésy, "Sensations on the skin similar to directional hearing, beats, and harmonics of the ear," *The Journal of the Acoustical Society of America*, vol. 29, no. 4, pp. 489–501, 1957.

[12] D. Goldreich, "A bayesian perceptual model replicates the cutaneous rabbit and other tactile spatiotemporal illusions," *PloS one*, vol. 2, no. 3, p. e333, 2007.

[13] A. Israr and I. Poupyrev, "Tactile brush: drawing on skin with a tactile grid display," in *Proceedings of the SIGCHI Conference on Human Factors in Computing Systems*, 2011, pp. 2019–2028.

[14] B. E. Treeby and B. T. Cox, "Modeling power law absorption and dispersion for acoustic propagation using the fractional laplacian," *The Journal of the Acoustical Society of America*, vol. 127, no. 5, pp. 2741–2748, 2010.

[15] J. Achenbach, *Wave propagation in elastic solids*. Elsevier, 2012.

[16] S. Holm, *Waves with power-law attenuation*. Springer, 2019.

[17] J. Garnier and M. Fink, "Super-resolution in time-reversal focusing on a moving source," *Wave Motion*, vol. 53, pp. 80–93, 2015.

[18] D. Goetz, G. Reardon, M. Linnander, and Y. Visell, "Dynamic feedback in wave-mediated surface haptics: A modular platform," *In Review*, 2023.

[19] G. Reardon, B. Dandu, Y. Shao, and Y. Visell, "Shear shock waves mediate haptic holography via focused ultrasound," *Science Advances*, vol. 9, no. 9, p. eadf2037, 2023.